Chapter 2

Characterization of Laser-Induced Defects and Modification in Carbon Nanotubes by Raman Spectroscopy

Masaru Tachibana

Additional information is available at the end of the chapter

http://dx.doi.org/10.5772/52091

1. Introduction

Defects in single-wall carbon nanotubes (SWCNTs) have a great influence on their physical properties. In real SWCNTs, various types of defects such as vacancies, Stone–Wales defects, adatoms, or H–C complex are contained as shown in Figure 1. Such defects can be introduced at the stage of SWCNT growth or later on during device or composite production. They can be also created deliberately by chemical treatment or by irradiation with electron, ion, or laser light. Understanding the properties of such defects in SWCNTs is important for improving SWCNT growth methods, tailoring their physical properties, and controlling the irradiation-induced damages.

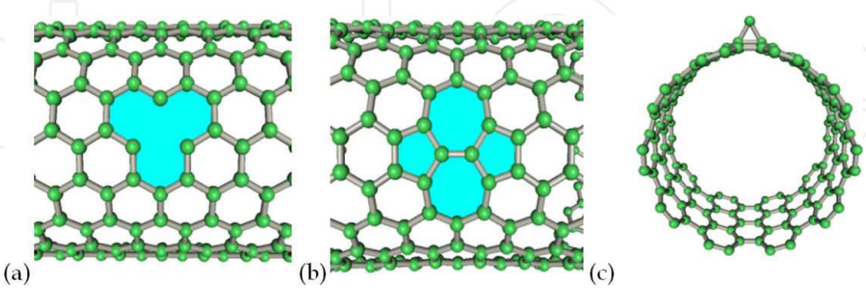

Figure 1. Schematic figures of typical defects such as (a) vacancy, (b) Stone-Wales defect, and (c) adatom in SWCNTs.

The irradiation with electron, ion, or laser light has been widely used for the studies not only on the properties of defects but also on the modification of CNTs. The nice reviews on electron and ion irradiation-induced effects in CNTs have been already published by Kra-

sheninnikov *et al.* [1,2]. However, there are very few reviews on laser-induced defects. The laser irradiation can lead to the heating followed by burning. Such laser irradiation also gives rise to interesting effects such as the production of defects and the modification of CNTs [3-7]. This chapter presents our recent studies [8-11] on laser-induced effects in SWCNTs.

Resonant Raman spectroscopy is one of the most powerful tools for characterizing structural and electronic properties of SWCNTs [12]. In the Raman spectra, defect-induced phonon mode so-called D band is observed at around 1350 cm^{-1}. The intensity of the D band can be enhanced as the number of defects is increased in the SWCNT. Therefore, the D band has been used for the assessment of imperfection of SWCNTs and the understanding of the properties of their defects. Further finding Raman bands associated with defects can lead the Raman spectroscopy to a more effective tool for the characterization of defects.

This chapter presents our recent studies [8-11]on the characterization of laser-induced defects and modification in SWCNTs by Raman spectroscopy. This chapter consists of four parts as mentioned below: (1) Thermal relaxation of laser-induced defects in SWCNTs, (2) Phonon control in metallic SWCNTs by laser–induced defects, (3) Fine structure of D band related to laser-induced defects in SWCNTs, and (4) Formation of *trans*-polyacetylene from SWCNTs by laser irradiation.

2. Raman spectra of SWCNTs

The resonant Raman spectra of SWCNTs include two main features: a radial breathing mode (RBM) observed in the range of 50–350 cm^{-1} and a tangential mode (the so-called G band) observed in the range of 1450–1650 cm^{-1} [12].

The RBM is a signature for the presence of SWCNTs, and is observed as a peak or a multi-peak feature. In the RBM, as suggested by its name, all the C atoms are vibrating in the radial direction with the same phase, as if the tube are breathing. The atomic motion does not break the tube symmetry, that is, the RBM is a totally symmetric (A_1) mode. Since this particular vibrational mode only occurs in SWCNTs, it is used to distinguish SWCNTs from other sp^2 carbons such as graphite and graphene.

A very important characteristic is the RBM frequency (ω_{RBM}) dependence on the tube diameter (d_t):$\omega_{RBM} \propto 1/d_t$ [13]. Most of the RBM experiment results in the literature have been fitted with the relation:

$$\omega_{RBM} = A / d_t + B \tag{1}$$

with values for the parameters A and B varying widely from paper to paper. Thus, the RBM can give an easy and quick determination of the tube diameter. In addition, it is of important that the RBM peak intensity is a function of excitation energy. The RBM is in-

http://dx.doi.org/10.5772/52091

tense when the incident light or the scattered light is in resonance with the SWCNT optical transition energies.

The G band (where the notation G comes from graphite) is related to the in plane C–C bond stretching mode in graphite and graphene. The G band is the Raman signature for all the sp^2 carbon materials, and is observed as a peak or multi-peak feature. The G band in SWCNTs is a more complex spectral feature. Due to the folding of graphene sheet into the SWCNT and the symmetry breaking effects associated with the nanotube curvature, G band splits into G^+ and G^- which are related to atomic vibrations preferencially along (LO) and perpendicular (TO) to the tube (folding) axis, respectively, for semiconducting SWCNT. For metallic tubes, electron-phonon coupling softens the LO modes, so that G^+ and G^- are actually with TO and LO modes, respectively.

The G^- peak for metallic tubes is fitted by asymmetric and broad Breit-Wigner-Fano (BWF) line:

$$I(\omega)=I_0\frac{[1+(\omega-\omega_{BWF})/q\Gamma]^2}{1+[(\omega-\omega_{BWF})/\Gamma]^2} \tag{2}$$

where I_0, ω_{BWF}, Γ, and $1/q$ are intensity, renormalized frequency, broadening parameter, and the asymmetric parameter, respectively [14]. Note that $\omega_{BWF}$and 2Γ are called the peak frequency and full width at half maximum (FWHM) of the BWF line, respectively. As clarified from Equation (2), $1/q$ determines the departure of the line shape from a symmetric Lorentzian line and, therefore, $|1/q|$ is a measure of the degree of the BWF coupling. Thus the asymmetric and broad BWF line is commonly used to distinguish metallic SWCNTs from semiconducting SWCNTs as fitted with symmetric Lorentzian lines.

Actually, due to the symmetry breaking effects associated with the nanotube curvature, G band in SWCNT generates up to six Raman-allowed G-band peaks corresponding to two totally symmetric A_1 modes, two E_1 modes and two E_2 symmetry modes. Three of each exhibit LO or TO-like vibration. Due to the delocalization effect and special resonance conditions, the A_1 modes usually dominante the G-band spectra.

In addtion, in the Raman spectra in SWCNTs, defect-induced phonon mode so-called D band is often observed at around 1350 cm^{-1} [12].The D band is a Raman signature of disorder in sp^2 carbons materials. The intensity of the D band can be enhanced as the number of defects is increased in the SWCNT. The D band has been used for the assessment of imperfection of SWCNTs and the understanding of the properties of their defects.

3. Thermal relaxation of laser-induced defects in SWCNTs

3.1. Laser irradiation for SWCNTs synthesized by electric arc-discharge method

SWCNTs synthesized by an electric arc-discharge method were used for laser irradition experiments. As-grown SWCNTs were purified by heating at 350°C for 90 min in air. A sus-

pension of purified SWNTs in ethanol was prepared by ultrasonication. By drop-coating and air-drying the suspension, a SWCNT thin film was formed on a quartz substrate. The SWCNT film was irradiated with a 248 nm (~5.0 eV) pulsed KrF excimer laser in air. The irradiation fluence was approximately 3 J/(cm^2·pulse). The irradiation pulse number was selected to be only one because more than two pulses led to the breakdown of the SWCNTs.

3.2. Change in D band by laser irradiaton and thermal annealing

Figure 2 shows D and G bands in the Raman spectra for non-irradiated SWCNTs, irradiated SWNTs with a 248 nm pulsed excimer laser of 3 J/(cm^2·pulse) in air, and annealed SWCNTs at 673 K in a vacuum of 1 Pa for 240 min after the laser irradiation. The inset shows the close up of the D band. All of the spectra were normalized to the maximum intensity of the G band. Note that the Raman excitation was provided with a 532 nm (~2.33 eV) of a Nd:YVO4 laser where the laser power level in a focal spot of 1 μm in diameter on the sample was kept below 0.1 mW to prevent overheating the sample.

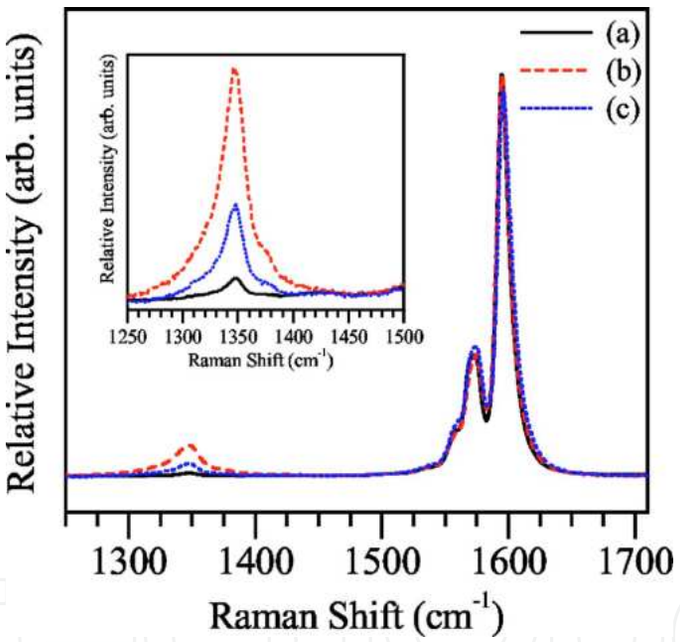

Figure 2. D and G bands in the Raman spectra of (a) pristine non-irradiated SWCNTs, (b) irradiated SWCNTs with a 248 nm pulsed excimer laser, and (c) annealed SWCNTs at 673 K for 240 min after the laser irradiation. The inset shows the close up of the D band. All of the spectra are normalized to the maximum intensity of the G band. [8]

It is found that the D band intensity significantly changes by laser irradiation and thermal annealing, while the spectral feature of the G band remains almost unchanged. For more clarifying the change in D band intensity, the relative intensity of the D band main peak at 1346 cm^{-1} to the G band main peak at 1593 cm^{-1} was defined as I_D/I_G. For non-irradiated SWCNTs as shown in Fig. 2(a), the $I_D/I_G$is 0.009. This value is very small and exhibits high quality SWCNTs. The I_D/I_Gsignificantly increases due to laser irradiation as seen in Fig. 2(b). The $I_D/I_G$for the irradiated SWCNTs is 0.08, which is about ten times as much as that

http://dx.doi.org/10.5772/52091

for the non-irradiated ones. Furthermore, when the irradiated SWNTs are thermally annealed at 673 K for 240 min, the I_D/I_G decreases and approaches that for non-irradiated ones as shown in Fig. 2(c). On the other hand, all peak frequencies, relative intensities, and FWHMs of RBM, D and G bands except for the intensity of the D band exhibit no significant change due to laser irradiation and thermal annealing. These spectral features mean that defects were successfully produced by the laser irradiation and relaxed by annealing with keeping the tubular structure of SWCNTs.

Let us consider the formation process of the laser-induced defects in SWCNTs. The knock-on energy of carbon atom into the direction perpendicular to the tube surface for an isolated SWCNT with a diameter over 1 nm is estimated to be 15–17 eV [15]. This energy is much higher than the irradiation energy of 248 nm (~5.0 eV) used in this experiment. This means that the formation of the laser-induced defects in SWCNTs would not be due to the physical knock-on phenomena. However, the increase of D band intensity related to the formation of defects clearly occurs for SWCNTs irradiated in air. The degree of the increase of D band intensity is much higher than those for SWCNTs irradiated in vacuum and Ar atmosphere. Therefore, the formation of the laser-induced defects in SWCNTs can be attributed to the chemical reaction with O_2 and H_2O in air by laser heating.

3.3. Analysis of recovery of D band by themal annealing

To examine the thermal relaxation of the laser-induced defects in SWCNTs, the time evolution of the relative intensity of D band in the irradiated samples at various annealing temperatures from 296 to 698 K was measured in the range of annealing times of 0 to 240 min. The typical annealing time evolution of the relative intensity of the D band at 573, 673, and 698 K are shown in Figure 3. Note that the *R* of the ordinate in the figure indicates the I_D/I_G normalized by that at *t*=0, i.e., before annealing for irradiated SWCNTs.

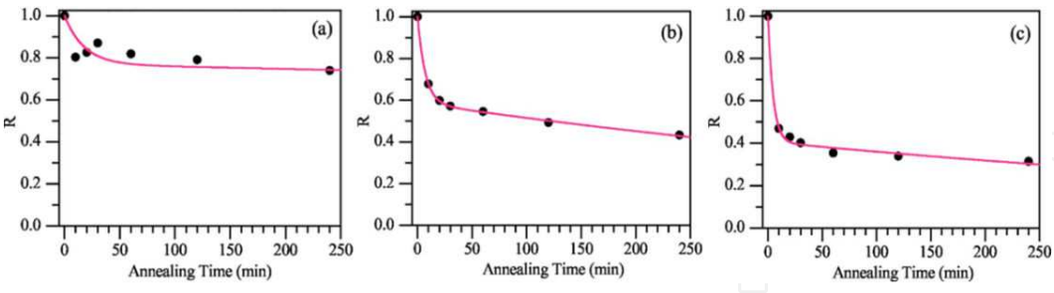

Figure 3. Time evolution of the *R* at annealing temperatures of (a) 573, (b) 673, and (c) 698 K for SWCNTs irradiated with a 248 nm pulsed excimer laser. Note that the *R* indicates the *ID*/ *IG* normalized by that at *t*=0, i.e., before annealing for the irradiated SWCNTs. Solid curves were obtained by the fitting analysis with Eq.(3). [8]

As shown in Fig. 3, the *R* decreases with increasing annealing time. For 573 K, the *R* gradually decreases and reaches 0.8 at 240 min. For 673 K, the *R* quickly decreases and reaches 0.6 at 20 min, and then slowly decreases and reaches 0.45 at 240 min. For 698 K, the *R* more quickly decreases and reaches 0.4 at 20 min, and then slowly decreases and reaches 0.3 at 240 min. On the other hand, no significant change in the *R* is observed for 296 K. These re-

sults indicate that the behavior of the R with annealing time strongly depends on annealing temperature. The feature of the dependence of the R on annealing time is clearly observed, especially at annealing temperatures of 673 and 698 K as shown in Figs. 3(b) and 3(c), respectively. From these behaviors, it is predicted that the thermal relaxation of laser-induced defects in SWCNTs includes two processes that have fast and slow rates.

As the previous analysis of the thermal relaxation kinetics of defects for graphite [16], the dependence of the R on annealing time for SWCNTs as shown in Fig. 3 was analyzed on the following three assumptions: (i) the I_D/I_G, or R is proportional to the density of defects in SWCNTs, (ii) some of the defects and others are annihilated by the fast and slow relaxation processes, respectively, and (iii) both processes occur independently. According to these assumptions, the annealing time evolution of the R can be expressed as

$$R(t) = A\exp(-k_I t) + (1 - A)\exp(-k_{II} t) \tag{3}$$

where A is the ratio of the defects relaxed by the fast relaxation process to the total defects in SWCNTs, k_I and k_{II} are the rate constants for the fast and slow relaxation processes, respectively, and t is annealing time. So the first and second terms on the right-hand side of Equation(3) correspond to the fast and slow relaxation processes, respectively. The annealing time evolution of the R as shown in Fig. 3 was fitted with Eq. (3). The fitted curves are indicated as solid lines in Fig. 3. As a result, the rate constants of k_I and k_{II} for the fast and slow relaxation processes, respectively, are determined as shown in Table I. For 296 K, k_I and k_{II} are estimated to be quite small ($<10^{-6}$) since no clear change in R was observed. The value of A runs from 0.23 through 0.59. As presented in Table I, both k_I and k_{II} show the strong temperature dependence.

Temperature (K)	k_I (s^{-1})	k_{II} (s^{-1})
296	$< 10^{-6}$	$< 10^{-6}$
573	9.5×10^{-4}	2.5×10^{-6}
623	1.5×10^{-3}	5.6×10^{-6}
648	2.9×10^{-3}	1.6×10^{-5}
673	2.4×10^{-3}	2.2×10^{-5}
698	3.5×10^{-3}	2.0×10^{-5}

Table 1. Thermal relaxation rate constants of k_I and k_{II} for the fast and slow processes, respectively, at annealing temperatures from 296 to 698 K for SWCNTs irradiated with a 248 nm pulsed excimer laser.[8]

3.4. Activation energies of thermal relaxation of laser-induced defects

Arrhenius plots of thermal relaxation rate constants of $k_I t$ and $k_{II} t$ in Table I are shown in Figure 4. From the slopes in Fig. 4, the activation energies for the fast and slow relaxation processes are determined to be 0.4 and 0.7 eV, respectively. According to the simulation on defects in

http://dx.doi.org/10.5772/52091

SWCNTs, the activation energy of the vacancy migration along the tube axis is calculated to be about 1 eV [17]. This value is close to that for the slow relaxation process as determined experimentally above. Such vacancy migration would also lead to the annihilation of the vacancies at the nanotube ends. Therefore, it is concluded that the slow relaxation process observed in this experiment corresponds to the vacancy migration along the tube axis.

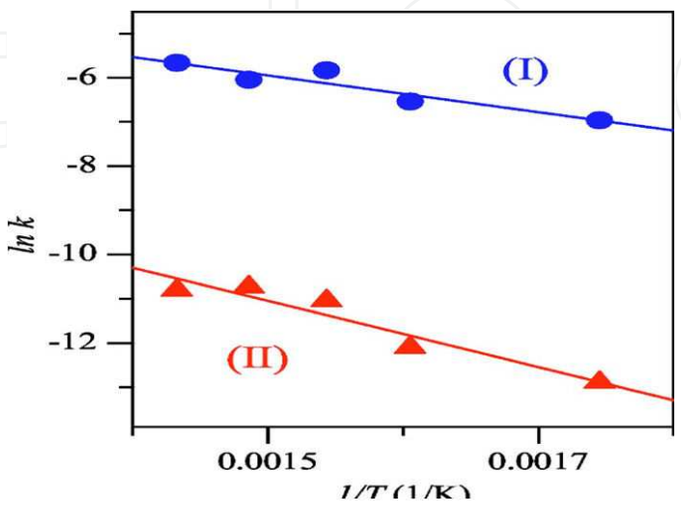

Figure 4. Arrhenius plots of the thermal relaxation rate constants of k_I(circles) and k_{II} (triangles) for the fast and slow processes, respectively, for SWCNTs irradiated with a 248 nm pulsed excimer laser, where T is the annealing temperature. [8]

On the other hand, two such relaxation processes have also been reported for graphite irradiated with He+ ions [16]. According to the report, the fast and slow relaxation processes correspond to the vacancy-interstitial recombination and vacancy migration in the graphene plane, respectively, which have the activation energies of 0.89 eV and 1.8 eV. This suggests that the slow relaxation process corresponds to the vacancy migration in both SWCNT and graphite. The activation energy of 0.7 eV of the vacancy migration for SWCNTs as deterimined experimentally above is much smaller than 1.8 eV for graphite. This smaller value for SWCNTs would be due to the curvature effect of nanotube that breaks the trigonal symmetry of a perfect graphene sheet. It is expected that, due to the curvature effect of nanotube, the activation energy of the vacancy-interstitial recombination for SWCNTs is also smaller than 0.89 eV for graphite. Thus, it is suggested that the fast relaxation process with the activation energy of 0.4 eV as determined in this experiment corresponds to the vacancy-interstitial recombination in SWCNTs.

In summary, laser-induced defects in SWCNTs can be introduced by the irradiation with a 248 nm pulsed excimer laser. The formation of defects might be related to thermal oxidation and burning by laser heating. Such laser-induced defects are thermally relaxed with two processes with fast and slow rates. The two relaxation processes show the strong temperature dependence. The activation energies of the fast and slow relaxation processes are determined to be 0.4 and 0.7 eV, respectively. These processes can correspond to vacancy-interstitial recombination and vacancy migration along the tube axis. Such relaxation

processes with fast and slow rates for SWCNTs are similar to those for graphite irradiated with He+ ions. However, their activation energies for SWCNTs are smaller than those for graphite. The smaller activation energies for SWCNTs would be due to the effect of curvature of nanotube.

4. Phonon control in metallic SWCNTs by laser–induced defects

4.1. Change in G band for metallic nanotubes by laser irradiation and thermal annealing

SWCNT samples after laser irradiation and themal annealing were prepared by similar procedure as described in 3.1. Figure 5 show D and G bands in Raman spectra for (a) pristine SWCNTs, (b) laser-irradiated SWCNT swith a 248 nm (~5.0 eV) pulsed KrF excimer laser of approximately 5 J/(cm^2 ·pulse), and (c) annealed SWNTs at 400 °C in a vacuum of ~9 Pa for 60 min after the irradiation. Note that the spectra excitation was provided with a 632.8 nm (~1.96 eV) of a He–Ne laser where the laser power level in a focal spot of 1 μm in diameter on the sample was kept below 0.1 mW to prevent overheating the samples.

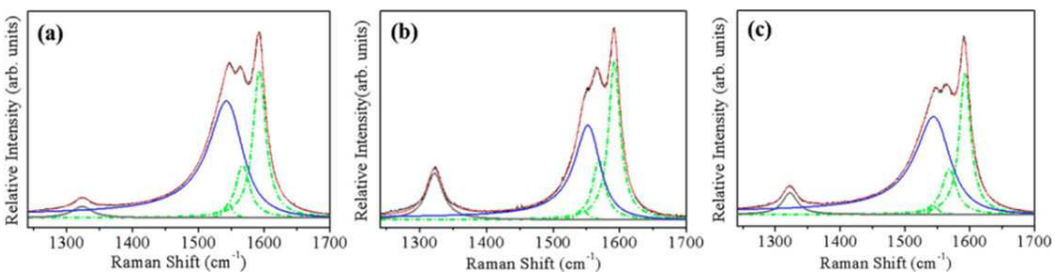

Figure 5. D and *G* bands in Raman spectra for (a) pristine SWNTs, (b) laser-irradiated SWNTs, and (c) annealed SWNTs after the irradiation, taken at E_{exc}=1.96 eV (λ_{exc}=632.8 nm). The *D* band was fittedwith one Lorentzian line. The *G* band was fitted with two Lorentzian (dotted) lines and one BWF (solid) line. [9]

D band was fitted with one Lorentzian line. On the other hand, G band was fitted with two Lorentzian lines and one asymmetric line that is Breit–Wigner–Fano (BWF) line [13] as given by Eq. (2). The values of the fitting parameters are listed in Table 2. In the G band for pristine SWCNTs in Fig. 5(a), one Lorentzian line at 1593 cm^{-1} corresponds to G^+ peaks for semiconducting SWCNTs and metallic SWCNTs. Note that G^+ peak associated with semiconducting SWCNTs is assumed to overlap with that with metallic ones. The other Lorentzian line at 1567 cm^{-1} corresponds to G^- peak associated with semiconducting SWCNTs. The asymmetric and broad line at 1546 cm^{-1} corresponds to G^- peak associated with metallic SWCNTs, which is largely downshifted, relative to G^+ one. These spectral components of the G band suggest that both semiconducting and metallic SWCNTs are resonant in the Raman spectrum of pristine SWCNTs taken with 1.96 eV in Fig. 5(a).

The D band for pristine SWCNTs was fitted with one Lorentzian curve at 1323 cm^{-1}. It is known that the intensity of the D band increases as the number of defects in SWCNTs is increased. The intensity ratio of D/G^+ peaks is often used as a measure of the defect density in

SWNTs. The relative intensity of the D band for pristine SWCNTs is 0.12. This value is quite small, comparable to those of high quality SWCNTs as reported so far. Thus, pristine SWCNTs used in this experiment have high quality or quite low defect density.

	pristine SWCNTs			laser-irradiated SWCNTs			annealed SWCNTs		
	ω (cm^{-1})	Γ (cm^{-1})	$I/I_{G^+(S+M)}$	ω (cm^{-1})	Γ (cm^{-1})	$I/I_{G^+(S+M)}$	ω (cm^{-1})	Γ (cm^{-1})	$I/I_{G^+(S+M)}$
G^+(S+M)	1593	24	1.0	1592	21	1.0	1593	21	1.0
G^-(S)	1567	26	0.36	1568	23	0.38	1568	27	0.33
G^-(M)	1546	63	0.78	1554	47	0.59	1548	65	0.69
D	1323	38	0.12	1322	31	0.42	1322	28	0.20

Table 2. Peak frequencies (ω), full widths at half maximum (Γ), and relative intensities ($I/I_{G^+(S+M)}$) of Lorentzian lines and Breit-Wigner-Fano lines used to fit D and G bands for pristine SWCNTs, laser-irradiated SWNTs, and annealed SWCNTs after the irradiation in Fig. 5. The relative intensities of the peaks are normalized by G^+ intense peak located at highest frequency. S and M indicate G peaks associated with semiconducting and metallic SWCNTs, respectively.

A significant change in the Raman spectrum was observed for laser-irradiated SWCNTs, as shown in Fig. 5(b). The intensity of the D band increased with the laser irradiation. Note that the frequency and linewidth remained almost unchanged even after the irradiation. These results mean that some specific defects were introduced in SWCNTs by the laser irradiation. The formation of defects might be related to thermal oxidation and burning by laser heating as discussed in 3.2. Moreover, it should be noticed that not only D band but also G band were affected by the laser irradiation. Especially, a significant change was observed for G^- peak associated with metallic tubes. The frequency of the G^- peak was upshifted by 8 cm^{-1}. Correspondingly, the linewidth of the G^- peak was reduced by 25%. In addition, the intensity ratio of the G^-/G^+ peak was reduced by 25%. On the other hand, the frequency, linewidth, relative intensity of G− peak associated with semiconducting SWCNTs remained almost unchanged even after the laser irradiation. Such behavior in the G^- peak associated with semiconducting SWCNTs is consistent with that in the G^- peak for the same SWCNTs taken with 2.33 eV in which only semiconducting SWNTs are resonant. Thus, the laser-induced defects significantly affect G^- peak associated not with semiconducting SWCNTs but metallic ones.

The G^- peak associated with metallic SWCNTs is due to the electron-phonon coupling as described in 2 [18,19]. The upshift of the frequency, the narrowing of the linewidth, and the reduction in the relative intensity for the G^- peak associated with metallic SWCNTs as seen in Fig. 5(b) imply the breaking of the electron-phonon coupling. Moreover, it should be noticed that D and G bands for the irradiated SWNTs recover the original ones after annealing in a vacuum of ~9 Pa at a sample temperature of 400 °C for 60 min, as shown in Fig. 5(c). As described in 3.4, the laser-induced defects such as vacancies can be annihilated by vacancy-interstitial recombination and vacancy migration to the nanotube end

due to the thermal annealing [8]. Such annihilation of vacancies can be responsible for the recovery of the Raman spectral profile. Thus, the electron-phonon coupling can be reversibly controlled by the generation and annihilation of specific defects due to laser irradiation and thermal annealing.

4.2. Change in RBM for metallic nanotubes by laser irradiation and themal annealing

The change corresponding to that in D and G bands in Fig. 5 was also observed for radial breathing modes (RBMs) at the range of 150–200 cm^{-1} in Raman spectra for pristine SWNTs, laser-irradiated SWCNTs, and annealed SWCNTs after the irradiation, taken with E_{exc} =1.96 eV(λ_{exc}=632.8 nm), as shown in Figure 6. The RBMs are actually composed of a lot of peaks corresponding to various kinds of chiralities or diameters of SWNTs. For simplifying, the RBMs were fitted with five Lorentzian lines. The values of the fitting parameters are listed in Table 3.

The diameters d of SWCNTs resonantly contributing to the Raman spectrum for pristine SWCNTs in Fig. 6(a) are estimated to be d=1.44±0.2 nm from the corresponding RBM frequencies ω_{RBM} using the relation $\omega_{RBM}(cm^{-1}) = 234/d(nm) + 10$ [20], which has been found for typical SWCNT bundles. Moreover, according to the (revised) Kataura plot [21,22] with the excitation energy and SWCNT diameters estimated above, it is suggested that both semiconducting and metallic SWCNTs are resonant in the Raman spectrum in Fig. 6(a). Note that one RBM peak at the lowest frequency of 157 cm^{-1} is mainly associated with semiconducting ones whereas other four ones at higher frequencies of 168, 173, 186, and 196 cm^{-1} are associated with metallic ones. This result is consistent with the result of spectral components in G band as discussed in 4.1.

The RBM peaks associated with metallic SWCNTs changed after the irradiation, as shown in Fig. 6(b). Especially, the most intense RBM peak at 173 cm^{-1} drastically decreased with the irradiation. On the other hand, no significant change was observed for only RBM peak at 157 cm^{-1} associated with semiconducting SWCNTs. These results mean that the resonant off for the Raman excitation of 1.96 eV occurs for metallic SWCNTs. This also suggests that the change in the electronic structure for metallic SWCNTs occurs due to the laser-induced defects.

Vacancy defects can cause a bandgap opening in metallic SWCNTs due to the breaking of the symmetry [23,24]. Such metal-semiconductor transition has been also experimentally demonstrated by the measurements of electrical properties for metallic SWCNTs with the introduction of defects [25,26]. Therefore, the change in the electronic structure with the bandgap opening can be responsible for the resonant off for metallic SWCNTs. Such change in the electronic structure for metallic SWCNTs due to the laser-induced defects is also consistent with the change in the corresponding G^- band, i.e., the breaking of the electron-phonon coupling, as discussed in 4.1.

Moreover, as seen in Fig. 6(c), the thermal annealing also leads to the recovery of the RBMs to original ones, as D and G band in Fig. 5. This recovery can be also explained by that in the electronic structure due to the thermal annihilation of laser-induced defects such as vacancies as discussed in 3.4.

http://dx.doi.org/10.5772/52091

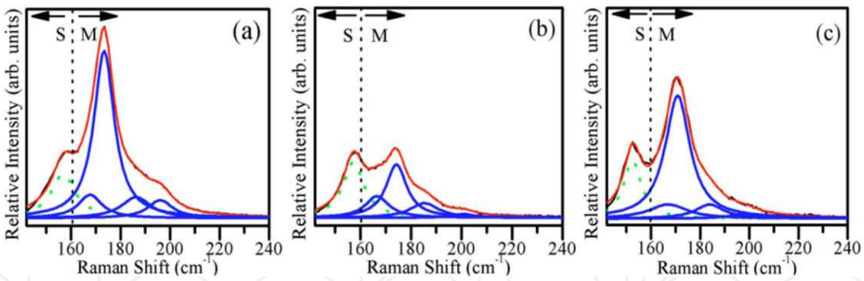

Figure 6. RBMs in Raman spectra for (a) pristine SWCNTs, (b) laser-irradiated SWCNTs, and (c) annealed SWCNTs after the irradiation, taken with E_{exc}=1.96 eV(λ_{exc}=632.8 nm). The RBMs were fitted with five Lorentzian lines. One (dotted) line at the lowest frequency is associated with semiconducting SWCNTs. Other (solid) lines at higher frequencies are associated with metallic SWCNTs. [9]

In summary, laser-induced defects influence not only D band but also G^- peak associated with metallic SWCNTs, which is attributed to the electron-phonon coupling with Kohn anomaly. The upshift and narrowing of the G^- peak occur due to the laser irradiation. The G^- peak can recover to the original one due to the thermal annealing. The electron-phonon coupling for metallic SWCNTs can be reversibly controlled by the generation and annihilation of specific defects due to the laser irradiation and thermal annealing.

	pristine SWNTs			laser-irradiated SWNTs			annealed SWNTs		
	ω (cm^{-1})	Γ (cm^{-1})	I/I_{S1}	ω (cm^{-1})	Γ (cm^{-1})	I/I_{S1}	ω (cm^{-1})	Γ (cm^{-1})	I/I_{S1}
S1	157	12	1.0	157	10	1.0	152	9	1.0
M1	168	12	0.52	167	11	0.43	167	19	0.53
M2	173	10	3.2	174	10	0.95	171	12	3.0
M3	186	15	0.59	185	14	0.36	184	14	0.40
M4	196	12	0.42	201	10	0.07	198	14	0.13

Table 3. Peak frequencies (ω), full widths at half maximum (Γ), and relative intensities (I/I_{S1}) of Lorentzian lines used to fit radial breathing modes (RBMs) for pristine SWCNTs, laser-irradiated SWCNTs, and annealed SWCNTs after the irradiation in Fig. 6. The relative intensities of the peaks are normalized by one located at lowest frequency associated with semiconducting SWCNTs. S and M indicate RBM peaks associated with semiconducting and metallic SWCNTs, respectively.

5. Fine structure of D band related to laser-induced defects in CoMoCAT SWCNTs

5.1. Heating and laser irradiation for CoMoCAT SWCNTs

As-received CoMoCAT SWCNTs (SWeNT® CG 100, SouthWest NanoTechnologies, Inc.) were used for heating and laser irradiation experiments. A suspension of SWCNTs in ethanol was prepared by ultrasonication. By drop-coating and air-drying the suspension, a SWCNT thin film was formed on a quartz substrate. For heating experiments, the film sam-

ples were annealed at 350 °C for 90 min in air. For laser irradiations, the samples were irradiated with a 532 nm (~2.33 eV) from a Nd:YVO_4 laser for 180 min. The irradiation power level in a focal spot of 1 μm in diameter on the sample was kept at ~20 mW. The heating and laser irradiation experiments were also carried out in a vacuum of~4.5 Pa and a dynamic vacuum of ~3.5×10^{-4} Pa, respectively.

5.2. Change in D band by heating

Figure 7 shows D and G bands in the Raman spectrum for a pristine CoMoCAT SWCNT sample. The corresponding radial breathing modes (RBMs) are also shown in the inset in the figure. Note that the spectrawere taken with E_{exc}=2.33 eV(λ_{exc}=532 nm) where the laser power level in a focal spot of 1 μm in diameter on the sample was kept below 0.1 mW to prevent overheating the sample.The spectral peaks are fitted with Lorentzian lines. From the RBM frequencies, the mean diameter of pristine SWCNTs is estimated to be ~0.8 nm, which corresponds to typical mean diameter of CoMoCAT ones [27]. Note that the diameter is estimated using ω [cm^{-1}]=234/d [nm]+10 where d is the SWCNT diameter and ω is the RBM frequency [12]. As shown in Fig. 7, the D band in pristine SWCNTs is fitted with two Lorentzian lines at 1313 and 1355 cm^{-1} which are denoted by D_1 and D_3, respectively. The relative intensities of the D components to the most intense G peak at 1594 cm^{-1} in each spectrum are compared in order to clarify the change in the D band.

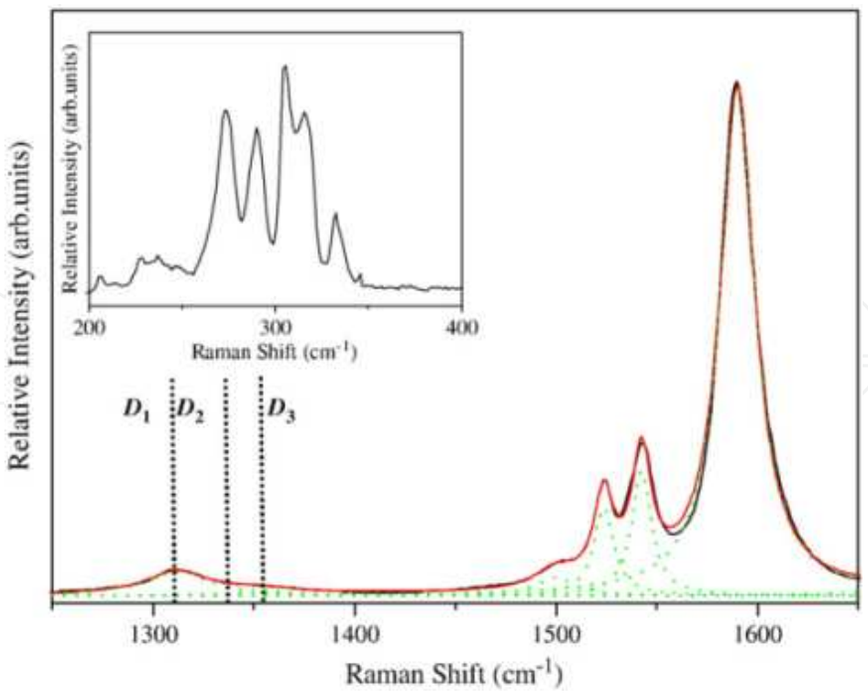

Figure 7. D and G bands in the Raman spectrum for a pristine CoMoCAT SWCNT sample. The corresponding radial breathing modes (RBMs) are also shown in the inset. [10].

http://dx.doi.org/10.5772/52091

Figure 8 shows *D* and *G* band in Raman spectra for CoMoCAT SWCNT samples heat-treated at 350 °C for 90 min in (a) air and (b) a vacuum of 4.5 Pa. The corresponding radial breathing modes (RBMs) are also shown in the inset. Note that these spectra were taken with E_{exc}=2.33 eV where the laser power level in a focal spot of 1 μm in diameter on the sample was kept below 0.1 mW to prevent overheating the sample. As shown in Fig. 8(a), the heat-treatment in air leads to the significant increase of the relative intensity of the D_3 component. The corresponding change is also seen in *G* band and RBMs. The broadening of *G* band occurs. This means that the imperfection of SWCNTs increases. Namely, a lot of defects are introduced into SWCNTs. In addition, the higher frequency peaks in the RBMs are disappeared. This means that the degradation of SWCNTs with smaller diameters occurs. On the other hand, no significant change in these Raman bands is observed in SWCNTs heat-treated in a vacuum of ~4.5 Pa as shown in Fig. 8(b). Therefore, it is suggested that the change in the Raman bands by the heat-treatment in air is due to the thermal oxidation.

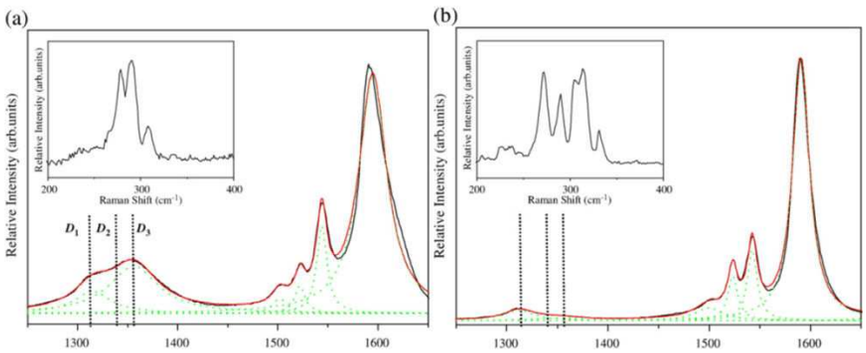

Figure 8. D and G bands in Raman spectra for CoMoCAT SWCNT samples heat-treated at 350 °C for 90 min in (a) air and (b) a vacuum of ~4.5 Pa. The corresponding radial breathing modes (RBMs) are also shown in the inset. [10]

Actually, pristine SWCNT sample contains impurities such as amorphous carbon, water, and C–H complex. The thermal oxidation gives rise to open-end structures of SWNTs or holes in the walls [28]. The extension of the oxidation process can generate C=O, C–O–C, and C–OH [29]. In addition, the corresponding *D* band frequency is theoretically predicted to be more than 1353 cm^{-1} [29]. This value is in good agreement with 1355 cm^{-1} of D_3. Thus, the D_3 component can be related to defects such as amorphous carbon and oxides as discussed above.

5.3. Change in D band by laser irradiation

Figure 9 shows *D* and *G* bands in Raman spectra for CoMoCAT SWCNT samples irradiated with E_{laser}=2.33 eV from a Nd:YVO_4 laser with 183 kW/cm^2-for 180 min in (a) air and (b) a dynamic vacuum of~3.5×10^{-4} Pa. The corresponding radial breathing modes (RBMs) are also shown in the inset. Note that these spectra were also taken with E_{laser}=2.33 eV where the laser power level in a focal spot of 1 μm in diameter on the sample was kept below 0.1 mW to prevent overheating the sample. As shown in Fig. 9(a), the laser irradiation in air leads to the increases of the relative intensities of not only D_3 but also D_1. The increase of the D_3 is

due to the thermal oxidation, similar to that by the heat-treatment in air as discussed in 5.2, since the laser irradiation occurs the local heating. It should be noted that the D_1 intensity increases by 78%, relative to the pristine one. However, no significant change is seen in *G* and RBMs. This means that no significant degradation of SWCNTs occurs. These behaviors are quite different from those by the heat-treatment in air as discussed in 5.2. In the laser irradiation in air, H_2 and O_2 radical species can be produced [29,30]. These with water can give rise to C–H complex on the side walls, at defect sites, or ends of SWCNTs [30,31]. Therefore, the D_1 can be related to C–H complex produced by the laser irradiation in air.

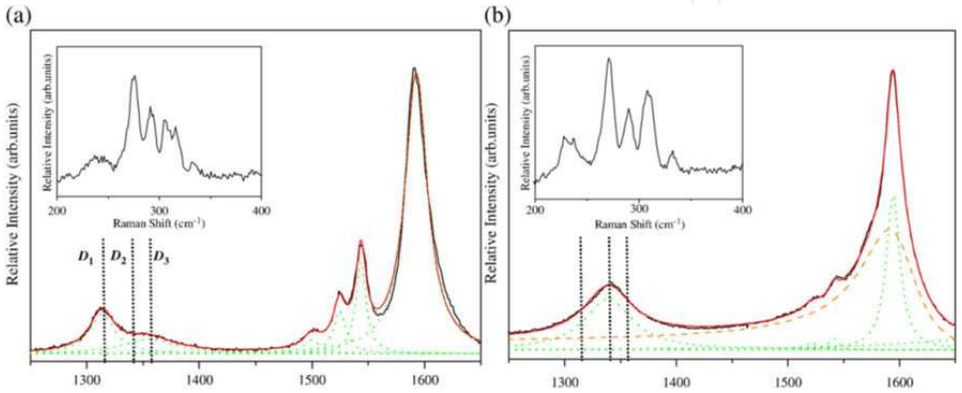

Figure 9. D and G bands in Raman spectra for CoMoCAT SWCNT samples irradiated with E_{laser}=2.33 eV from a Nd:YVO laser for 180 min in (a) air and (b) a dynamic vacuum of~3.5×10^{-4} Pa. The corresponding radial breathing modes (RBMs) are also shown in the inset.[10]

On the other hand, the laser irradiation in a dynamic vacuum of ~3.5×10^{-4} Pa leads to the appearance of a new *D* component at ~1340 cm^{-1}, denoted by D_2, as shown in Fig. 9(b). The peak profile is quite similar to that of step edges in graphite [32]. Therefore, the D_2would be related to the edges of SWCNTs cut by the laser irradiation in the dynamic vacuum. Such cutting might be due to absorbates-assisted burning by laser heating. In addition, it is of interest that the decrease of the D_1 intensity, relative to the pristine one, is observed. The C–H complex formed on SWCNTs is released by thermal annealing at more than 200 °C [30]. The laser irradiation in this experiment gives rise to the local heating. This will lead to the dehydration of SWCNTs so that the D_1 intensity can be decreased. The dehydration is also accompanied by the increases of the intensities of thelower frequency peak at 230 cm^{-1} in the RBMs and of the broad Breigt–Wigner–Fano line in the *G* band, associated with metallic SWCNTs, as seen in Fig. 9(b).

In summary, *D* band in CoMoCAT SWCNTs is composed of three components D_1, D_2, and D_3 at ~1313, 1340, and 1355 cm^{-1}, respectively. These components are attributed to different kinds of defects introduced by heating and laser irradiation. Such insight on the fine structure of the *D* band will play a role for more detailed understanding of *D* band and the identification of defects in SWCNTs.

http://dx.doi.org/10.5772/52091

6. Formation of *trans*-polyacetylene from CoMoCAT SWCNTs by laser irradiation

6.1. Laser irradiation for CoMoCAT SWCNTs

As-received CoMoCAT SWCNTs (SWeNT@CG 100, SouthWest NanoTechnologies, Inc.) were used in this experiment. A suspension of SWCNTs in ethanol was prepared by ultrasonication. The suspension was dropped on a clean quartz substrate and allowed to be air-dried at room temperature. The SWCNTs samples prepared in above procedure were used for laser irradiation experiments. The samples, which were exposed to air for less than 1 h before laser irradiation, are called "short air-exposure" ones. Some of samples were kept in air at room temperature for more than six months before laser irradiation. They are called ''long air-exposure'' ones.

Laser irradiation experiments were carried out using a micro-Raman systemequipped with mirrors, attenuators, a 100× microscope objective, a holographic notch filter, a single grating spectrometer (1800 1/mm grating), and a charge coupled device detector. In the laser irradiation experiments, all attenuators were removed. A 532 nm (~2.33 eV) from a cw Nd:YVO_4 laser was used to irradiate the samples. The laser beam was focused on the sample through the 100× microscope objective, with spot size of 1 μm. The laser power level on the sample was kept at 17.8 mW/μm^2. The irradiation time was 1 h.

6.2. Irradition effect for "short air-exposure" CoMoCAT SWCNTs

Figure 10 shows D and G bands in Raman spectra for a ''short air-exposure''CoMoCAT SWCNT sample (a) before and (b) after laser irradiation of a 532 nm with 17.8 mW/μm^2 for 1 h in air. The corresponding RBMs are also shown in the inset in the figure. Note that the spectra excitation was also provided with λ_{exc}=532 nm where the laser power level in a focal spot of 1 μm in diameter on the sample was kept below 0.2 mW/μm^2 to prevent overheating the sample.

The spectral peaks are fitted with Lorentzian lines. From the RBM frequencies in Fig. 10(a), the mean diameter of SWCNTs is estimated to be 0.8 nm, which corresponds to typical mean diameter of CoMoCAT ones [27]. Note that the diameter is estimated using ω [cm^{-1}] = 234/d [nm] + 10 where d is the SWCNT diameterand ω is the RBM frequency [20]. The D band at 1300–1400 cm^{-1} and G band at 1500–1700 cm^{-1} are associated with defects and tangential modes of SWCNTs, respectively. The D band can be fitted with two Lorentzian lines at 1313 and 1346 cm^{-1}. The G band can be fitted with three Lorentzian lines at 1523, 1543, and 1591 cm^{-1}.

After laser irradiation, the increase of relative intensity ofD band is observed as seen in Fig. 10(b). Especially, the lower-frequency component increases. The increase of D band intensity can be attributed to the oxidation and/or hydrogenationof SWCNTs [10,29,30] as discussed in 5. In addition, the RBMs exhibit the decrease of higher-frequency components by laser irradiation. This means that smaller diameter SWCNTs are degraded by thermal oxidation

due to laser heating. On the other hand, no significant change in G band is observed as seen in Fig. 10(b).

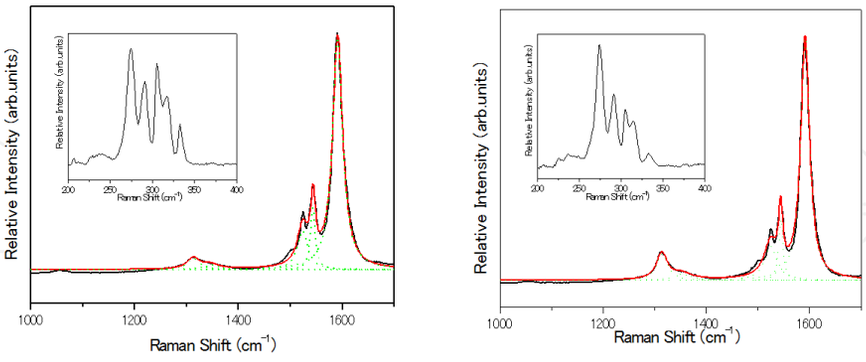

Figure 10. D and G bands in Raman spectra for a ''short air-exposure''CoMoCAT SWCNT sample (a) before and (b) after laser irradiation of a 532 nm with 17.8 mW/μm^2 for 1 h in air. The corresponding RBMs are also shown in the inset in the figure. [11]

6.3. Irradiation effect for "long air-exposure" CoMoCAT SWCNTs

Figure 11 shows D and G bands in Raman spectra for a ''long air-exposure''CoMoCAT SWCNT sample (a) before and (b) after laser irradiation of a 532 nm with 17.8 mW/μm^2 for 1 h in air. The corresponding RBMs are also shown in the inset in the figure.Note that the spectra excitation was also provided with λ_{exc}=532 nm where the laser power level in a focal spot of 1 μm in diameter on the sample was kept below 0.2 mW/μm^2 to prevent overheating the sample. As seenin Fig. 11(a), the ''long air-exposure'' sample also exhibits clearD and G bands, and RBMs, fitted by Lorentzian lines, as pristine ones. The peak profiles of G band and RBMs are similar to those of pristine one. On the other hand, the relative intensity of D band increases compared with that of pristine one in Fig. 10(a). The D band intensity is similar to that of the irradiated "short air-exposure'' one in Fig. 10(b). This means that the oxidation and/or hydrogenation occur in ''long air-exposure'' ones even before laser irradiation. This is due to the exposure of air with water vapor for the long time more than six months.

It should be noted that a significant change in Raman spectra is observed for the irradiated ''long air-exposure''sample as seen in Fig. 11(b). Namely, new intense peaks appearat 1138 cm^{-1} and 1514 cm^{-1} for the irradiated ''long air-exposure'' sample. These spectral features are quite similar to those of *trans*-polyacetylene, as have been reported so far [33–36]. According to the model calculation [37], the lower-frequency peak of 1138 cm^{-1} is assigned to a coupled C–C stretching and C–H bending vibration. The higher-frequency peak of 1514 cm^{-1} is assigned to a C–C stretching vibration. In addition, for short polyacetylene chains, the peak position around 1150 cm^{-1} strongly depends on the chain length, and shifts to lower frequency with increasing chainlength [37]. Thus, the appearance of intense peaks of 1138 and 1514 cm^{-1} means that *trans*-polyacetylene-like structural units are formed in irradiated ''long air-exposure''samples.

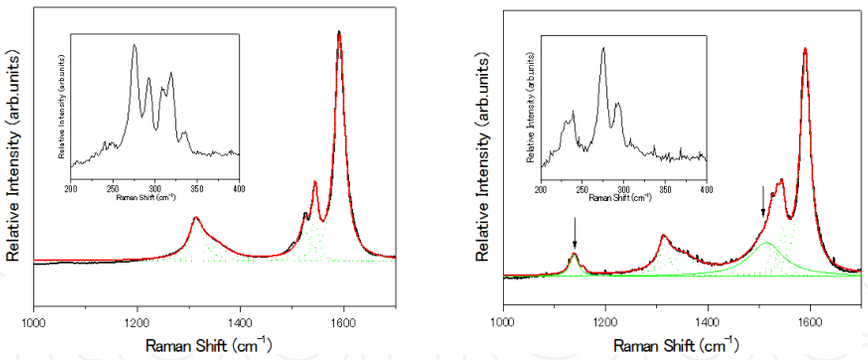

Figure 11. D and G bands in Raman spectra for a ''long air-exposure''CoMoCAT SWCNTsample (a) before and (b) after laser irradiation of a 532 nm with 17.8 mW/μm^2 for 1 h in air. The corresponding RBMs are also shown in the inset in the figure. The arrows indicate peaks at 1138 and1514 cm^{-1}associated with *trans*-polyacetylene. [11]

6.4. Formation of polyacetylene from SWCNTs

In ''long air-exposure'' samples, a lot of water vapor can be absorbed. To remove the absorbed water, the ''long air-exposure''samples were annealed at 150 °C for 1 h under a dynamic vacuum of 8.7×10^{-7} Pa. In order to examine the effect of absorbed water on the formation of *trans*-polyacetylene, laser irradiation experiments were also carried out for the annealed ''long air-exposure'' samples. As a result, for the annealed samples, no clear peak at around 1140 and 1540 cm^{-1} corresponding to *trans*-polyacetylene were appeared even after the laser irradiation. This means that the absorbed water plays a role for the formation of *trans*-polyacetylene.

Let us consider the formation process of *trans*-polyacetylene from ''long air-exposure'' samples by laser irradiation. It is well-known that CoMoCAT SWCNTs(SWeNT CG 100) include metal catalysts [27]. The catalysts are coated by a carbon layer, and deactivated. The water-can remove the carbon layer at high temperature, and revive the catalytic activity [38]. In ''long air-exposure'' samples used in this experiment, the water vapor can be sufficiently absorbed on catalysts. The water can remove the carbon layer under laser heating and revive catalytic activity. Consequently, as observed in graphite, graphene and CNT[39-43], the cutting of nanotubes can be realized by catalytic hydrogenation of carbon atoms, in which metal particle dissociate carbon atoms in CNTs, and then the dissociated carbon atoms react with H_2 to create hydrocarbon species such as CH_4. The cutting can be also accompanied with the formation of C–H species on the nanotubes as shown in Figure 12. Such cutting process would lead to the formation of polyacetylene-like structural units.

In summary, *trans*-polyacetylene is formed from CoMoCATSWCNT samples including metal catalysts and absorbed water by laser heating in air. The formation process might be related to the cutting of SWCNTs due to the catalytic hydrogenation of carbon atoms with laser heating, although the detailed mechanism is not yet understood. This shows a new use of the laser irradiation for the formation of functional materials from SWCNTs.

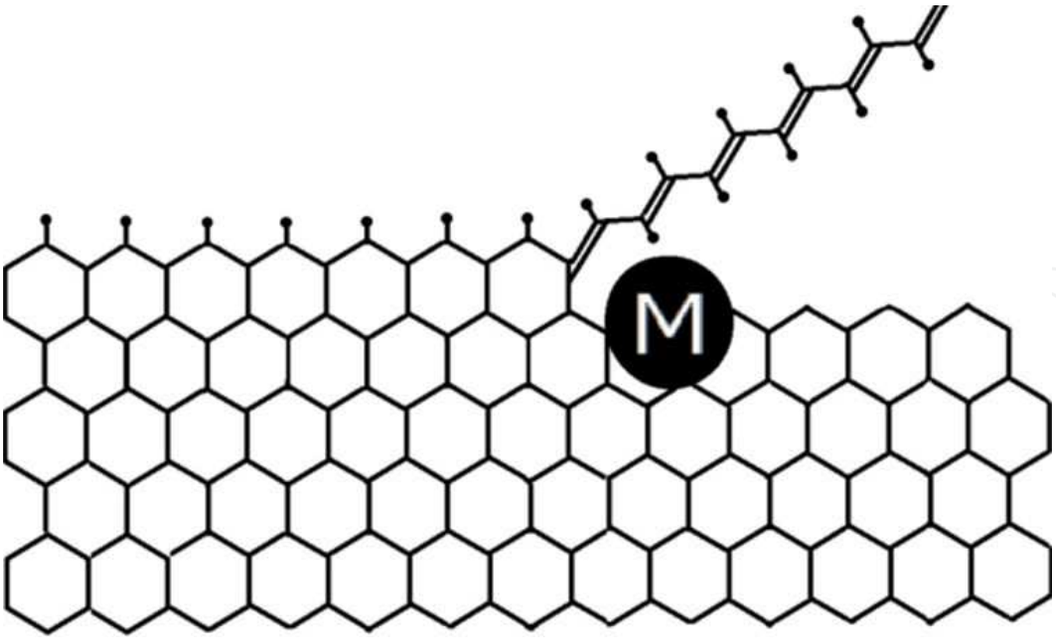

Figure 12. Schematic drawing of the formation of *trans*-polyacetylene by the cutting of SWCNT edge due to the catalytic hydrogenation with laser irradiation.

7. Summary

This chapter presented the characterization of laser-induced defects in SWCNTs by Raman spectroscopy. The laser irradiation with heating followed by burning can produce defects such as vacancies and interstitials in SWCNTs. These defects greatly influence electronic structures and phonon properties especially in metallic nanotubes. They can also be thermally relaxed by vacancy-interstitial recombination and vacancy migration along the tube axis with activation energy of 0.4 eV and 0.7 eV, respectively. This means that the electronic structures and phonon properties in metallic nanotubes can be reversibly controlled by the generation and annihilation of specific defects due to laser irradiation and thermal annealing. In addition, it was presented that the fine structure of Raman D band can be related to specific defects such as C-H complex on nanotubes and nanotube edges produced by laser irradiation. This can lead the Raman spectroscopy to a more effective tool for the characterization of defects in SWCNTs. Finally, it was presented that the laser irradiation can give rise to the formation of trans-polyacetylene from SWCNTs. The formation process might be related to the cutting of SWCNTs due to the catalytic hydrogenation of carbon atoms with laser heating, although the detailed mechanism is not yet understood. This shows a new use of the laser irradiation for the formation of functional materials from SWCNTs. Thus, the laser irradiation is useful for not only the understanding of the properties of defects in SWCNTs but also the modificaton of SWCNTs, as electron and ion irradiations.

http://dx.doi.org/10.5772/52091

Acknowledgements

The author acknowledges the contributions to the works presented here by all past and present collaborators, especially Dr. Takashi Uchida, Dr. Hironori Kawamoto, Mr Ken-ichi Kato, Mr. Dongchul Kang, Ms. Mari Hakamatsuka, Ms. Nagisa Hosoya, Mr. Noriaki Nemoto, and emeritus Prof. Kenichi Kojima. The works were supported in part by Strategic Research Projects in Yokohama City University and MEXT/JSPS KAKENHI.

Author details

Masaru Tachibana*

Address all correspondence to: tachiban@yokohama-cu.ac.jp

Department of Nanosystem Science, Yokohama City University, Japan

References

[1] Krasheninnikov, A. V., & Banhart, F. (2007). Engineering of nanostructured carbon materials with electron or ion beams. *Nat. Mater*, 6, 723-733.

[2] Krasheninnikov, A. V., & Nordlund, K. (2010). Ion and electron irradiation-induced effects in nanostructured materials. J. Appl. Phys , 107, 071301-1-70.

[3] Suzuki, S., & Kobayashi, Y. (2007). Healing of Low-Energy Irradiation-Induced Defects in Single-Walled Carbon Nanotubes at Room Temperature. *J. Phys. Chem. C*, 111(12), 4524-4528.

[4] Zandian, B., Kumar, R., Theiss, J., Bushmaker, A., & Cronin, S. B. (2009). Selective destruction of individual single walled carbon nanotubes by laser irradiation. *Carbon*, 47(5), 1292-1296.

[5] Jeschke, H. O., Diakhate, M. S., & Garcia, M. E. (2009). Molecular dynamics simulations of laser-induced damage of nanostructures and solids. *Applied Physics A: Materials Science & Processing*, 96(1), 33-42.

[6] Kumar, P., Panchakarla, L.S., & Rao, C.N.R. (2011). Laser-induced unzipping of carbon nanotubes to yield graphenenanoribbons. *Nanoscale*, 3, 2127-2129.

[7] Mases, M., Noël, M., Dossot, M., Mc Rae, E., & Alexander, V. (2011). Laser-induced damage and destruction of HiPCO nanotubes in different gas environments. *physica status solidi*, 248(11), 2540-2543.

[8] Uchida, T., Tachibana, M., & Kojima, K. (2007). Thermal relaxation kinetics of defects in single-wall carbon nanotubes. *J. Appl. Phys*, 101, 084313-1-4.

[9] Kang, D., Kato, K., Kojima, K., & Uchida, T. (2008). Tachibana M. Phonon control in metallic carbon nanotubes due to laser-induced defects. *Appl. Phys. Lett*, 93, 133102-1-3.

[10] Kang, D., Hakamatsuka, M., Kojima, K., & Tachibana, M. (2010). Influence of heating and laser irradiation on the Raman D band in single-wall carbon nanotubes. *Diamond & Related Materials*, 19, 578-580.

[11] Hakamatsuka, M., Yoshimura, H., & Tachibana, M. (2011). Formation of trans-polyacetylene from single-wall carbon nanotubes. *Carbon*, 46, 1869-1872.

[12] Jorio, A., Dresselhaus, M., Saito, R., & Dresselhaous, G. F. (2011). Raman Spectroscopy in Graphene Related Systems. *Weinheim: Wiley-VCH*.

[13] Bandow, S., Asaka, S., Saito, Y., Rao, A. M., Grigorian, L., Richte, E., & Eklund, P. C. (1998). Effect of the Growth Temperature on the Diameter Distribution and Chirality of Single-Wall Carbon Nanotubes. *Phys. Rev. Lett*, 80, 3779-3782.

[14] Brown, D. M., Jorio, A., Corio, P., Dresselhaus, M. S., Dresselhaus, G., Saito, R., & Kneipp, K. (2001). Origin of the Breit-Wigner-Fanolineshape of the tangential G-band feature of metallic carbon nanotubes. *Phys. Rev. B*, 63, 155414-155421.

[15] Crespi, V. H., Chopra, N. G., Cohen, M. L., Zettl, A., & Louie, S. G. (1996). Anisotropic electron-beam damage and the collapse of carbon nanotubes. *Phys.Rev. B*, 54, 5927-5931.

[16] Asari, E., Kitajima, M., Nakamura, K. G., & Kawabe, T. (1993). Thermal relaxation of ion-irradiation damage in graphite. *Phys. Rev. B*, 47, 11143-11148.

[17] Krasheninnikov, A. V., Lehtinen, P. O., Foster, A. S., & Nieminen, R. M. (2006). Bending the rules: Contrasting vacancy energetics and migration in graphite and carbon nanotubes. *Chem. Phys. Lett*, 418, 132-136.

[18] Lazzeri, M., Piscanec, S., Mauri, F., Ferrari, A. C., & Robertson, J. (2006). Phonon linewidths and electron-phonon coupling in graphite and nanotubes. *J. Phys. Rev. B*, 73, 155426-155431.

[19] Piscanec, S., Lazzeri, M., Robertson, J., Ferrari, A. C., & Mauri, F. (2007). Optical phonons in carbon nanotubes: Kohn anomalies, Peierls distortions, and dynamic effects. *Phys.Rev. B*, 75, 035427-035448.

[20] Milnera, M., Kurti, J., Hulman, M., & Kuzmany, H. (2000). Periodic Resonance Excitation and Intertube Interaction from Quasicontinuous Distributed Helicities in Single-Wall Carbon Nanotubes. *Phys. Rev. Lett*, 84, 1324-1327.

[21] Kataura, H., Kumazawa, Y., Maniwa, Y., Umezu, I., & Suzuki, S. (1999). Ohtsuka Y.,Achiba Y. Optical properties of single-wall carbon nanotubes. *Synth Met*, 103, 2555-2558.

[22] Jorio, A., Fantini, C., Pimenta, M. A., Capaz, R. B., Samsonidze, G. G., Dresselhaus, G., Dresselhaus, M. S., Jiang, J., Kobayashi, N., Gruneis, A., & Saito, R. (2005). Reso-

nance Raman spectroscopy (n,m)-dependent effects in small-diameter single-wall carbon nanotubes. *Phys. Rev. B*, 71, 075401-075411.

[23] Li, Y., Rotkin, S. V., & Ravaioli, U. (2004). Metal-semiconductor transition in armchair carbon nanotubes by symmetry breaking. *Appl. Phys. Lett*, 85, 4178-4180.

[24] , Y., Lehtinen, P. O., Foster, A. S., & Nieminen, R. M. (2004). Magnetic properties of vacancies in graphene and single-walled carbon nanotubes. *New J. Phys*, 6(68).

[25] Vijayaraghavan, A., Kanzaki, K., Suzuki, S., Kobayashi, Y., Inokawa, H., Ono, Y., Kar, S., & Ajayan, P. M. (2005). Metal–Semiconductor Transition in Single-Walled Carbon Nanotubes Induced by Low-Energy Electron Irradiation. *Nano Lett*, 5, 1575-1579.

[26] Park J.Y. (2007). Electrically tunable defects in metallic single-walled carbon nanotubes. *Appl. Phys. Lett*, 90(2), 023112-023114.

[27] Bachilo, S. M., Balzano, L., Herrera, J. E., Pompeo, F., Resasco, D. E., & Weisman, R. B. (2003). Narrow (n,m)-Distribution of Single-Walled Carbon Nanotubes Grown Using a Solid Supported Catalyst. *J. Am. Chem. Soc.*, 125(37), 11186-11187.

[28] Hou, P. X., Liu, C., & Cheng, H. M. (2008). Purification of carbon nanotubes. *Carbon*, 46(15), 2003-2025.

[29] Silva, A. M. D., Junqueira, G. M. A., Anconi, C. P. A., & Santos, H. F. D. (2009). New Insights on Chemical Oxidation of Single-Wall Carbon Nanotubes: A Theoretical Study. *Phys. Chem. C*, 113(23), 10079-10084.

[30] Zhang, G., Qi, P., Wang, X., Lu, Y., Mann, D., Li, X., & Dai, H. (2006). Hydrogenation and Hydrocarbonation and Etching of Single-Walled Carbon Nanotubes. *J. Am. Chem. Soc.*, 128(18), 6026-6027.

[31] Nikitin, A., Ogasawara, H., Mann, D., Denecke, R., Zhang, Z., Dai, H., Cho, K., & Nilsson, A. (2005). Hydrogenation of Single-Walled Carbon Nanotubes. *Phys. Rev. Lett.*, 95(22), 225507-225510.

[32] Cancado, L. G., Pimenta, M. A., Neves, B. R. A., Dantas, M. S. S., & Jorio, A. (2004). Influence of the Atomic Structure on the Raman Spectra of Graphite Edges. *Phys. Rev. Lett.*, 93(24), 247401-247404.

[33] Kuzmany, H., & Knoll, P. (1986). Resonance Raman cross-section and polarization of light scattered from trans-polyacetylene. *Raman Spectroscopy*, 17(1), 89-92.

[34] Takeuchi, H., Arakawa, T., Furukawa, Y., Harada, I., & Shirakawa, H. (1987). Density of vibrational states in trans-polyene: comparison with the infrared, Raman and neutron spectra of trans-polyacetylene. *J MolStruct*, 158, 179-193.

[35] Ferrari, A. C., & Robertson, J. (2001). Origin of the 1150-cm 1 Raman mode in nanocrystalline diamond. *Phys Rev B*, 63(12), 121405-121408.

[36] Kuzmany, H., Pfeiffer, R., Salk, N., & Günther, B. (2004). The mystery of the 1140 cm 1 Raman line in nanocrystalline diamond films. Carbon ., 42(5-6), 911-917.

[37] Owens F.J. (2005). Effect of nanosizing on some properties of one dimensional polyacetylene chains. *Physica E*, 25(4), 404-408.

[38] Yamada, T., Maigne, A., Yudasaka, M., Mizuno, K., Futaba, D. N., Yumura, M., Iijima, S., & Hata, K. (2008). Revealing the secret of water-assisted carbon nanotube synthesis by microscopic observation of the interaction of water on the catalysts. *Nano Lett*, 8(12), 4288-4292.

[39] Tomita, A., & Tamai, Y. (1974). An optical microscopic study on the catalytic hydrogenation of graphite. *J PhysChem*, 78(22), 2254-2258.

[40] Datta, S. S., Strachan, D. R., Khamis, S. M., & Johnson, A. T. C. (2008). Crystallographic etching of few-layer graphene. *Nano Lett.*, 8(7), 1912-1915.

[41] Campos, L. C., Manfrinato, V. R., Sanchez-Yamagishi, J. D., Kong, J., & Jarillo-Herrero, P. (2009). Anisotropic etching and nanoribbon formation in single-layer graphene. *Nano Lett.*, 9(7), 2600-2604.

[42] Ci, L., Song, L., Jariwala, D., Elías, A. L., Gao, W., Terrones, M., & Ajayan, P. M. (2009). Graphene shape control by multistage cutting and transfer. *Adv Mater.*, 21(41), 4487-4491.

[43] Elías, A. L., Botello-Méndez, A. R., Meneses-Rodríguez, D., González, V. J., Ramírez-González, D., Ci, L., Muñoz-Sandoval, E., Ajayan, P. M., Terrones, H., & Terrones, M. (2010). Longitudinal cutting of pure and doped carbon nanotubes to form graphitic nanoribbons using metal clusters as nanoscalpels. *Nano Lett.*, 10(2), 366-372.